One-pot synthesis of C/Bi/Bi$_2$O$_3$ composite with enhanced photocatalytic activity

Qiang Hao[a], Ruiting Wang[a], Haojie Lu[a], Ci'an Xie[a], Weihua Ao[a], Daimei Chen[a,*], Chao Ma[b], Wenqing Yao[b], Yongfa Zhu[b,*]

[a] Beijing Key Laboratory of Materials Utilization of Nonmetallic Minerals and Solid Wastes, National Laboratory of Mineral Materials, School of Materials Science and Technology, China University of Geosciences, Beijing, 100083, China
[b] Department of Chemistry, Tsinghua University, Beijing, 100084, PR China

ABSTRACT

In this work, a novel C/Bi/Bi$_2$O$_3$ composite photocatalyst was prepared by a facile one-pot method, using EDTA-Bi as a precursor. The C/Bi/Bi$_2$O$_3$ composite photocatalyst exhibited higher photocatalytic activity than Bi$_2$O$_3$ on the degradation of 2,4-dichlorophenol (2,4-DCP) under both simulated sunlight and visible light irradiation. Metallic Bi and the remaining organic carbon cannot only enhance the absorption of lights, but also accelerate the seperation of photogenerated charge carriers. As a result, the photocatalytic activity is enhanced. More importantly, this paper provides a facile method for the preparation of C/Bi/Bi$_2$O$_3$ composite materials, which is suitable for mass production.

© 2017 Published by Elsevier B.V.

1. Introduction

Traditional photocatalytic materials such as TiO$_2$ [1–4], ZnO [5–7] and BiPO$_4$ [8,9] have outstanding photocatalytic performance under ultraviolet light irradiation, while their band gaps are too wide to absorb visible light. In order to improve the utilization rate of solar light, researchers pay more attention to develop novel visible light responsed photocatalysts. Recently, some visible light responsed photocatalysts such as g-C$_3$N$_4$ [10–14], iron oxide [15,16], tungsten oxide [17,18], cuprous oxide [19,20]

Bi-based photocatalysts [21–24] etc, have attracted great interest of researchers for their various species, unique electronic structure, excellent visible light absorption ability and high degradation ability of organic compounds. However, due to the rapid recombine of photogenerated charge carries, their catalytic activity is not high.

Compared with other Bi-based photocatalysts, Bi$_2$O$_3$ is the most common Bi-based photocatalyst with a lot of advantages. For instance, it has a narrow band gap which can be excited by visible light, moreover, Bi$_2$O$_3$ is nontoxic and easy-prepared [25,26]. Bi$_2$O$_3$ has four kinds of crystal forms, which are the monoclinic form, the tetragonal form, the body-centered cubic form and the face-centered cubic form. Among them, the monoclinic bismuth oxide is the stablest and the most likely to be applied in the treatment of waste water [27]. However, the band gap around 2.7 eV indicates that Bi$_2$O$_3$ can only utilize a small amount of solar energy, Moreover, photogenerated electron-hole pairs can easily recombine and the photo quantum efficiency of Bi$_2$O$_3$ is not high, so the photocatalytic performance of bismuth oxide is still not ideal [28]. Another reason is that grain size of Bi$_2$O$_3$ is often too large for interface reaction [35].

Several methods and techniques have been employed to modify Bi$_2$O$_3$ [28–30,34–36]. Creating heterjunctions with other semiconductors, such as ZnO, SrFe$_{12}$O$_{19}$, BiOI et al. can improve the photocatalytic activity of Bi$_2$O$_3$ [28–30]. In this method, finding a matched crystal lattice is a conundrumo. Besides, other semiconductors must be introduced to the composites and it is quite costed and the preparation methods are complex. Surface plasmon resonance (SPR) effect of noble metal is considered as a crucial way for the enhancement of photocatalytic efficiency. Au, Ag and Pt have been widely reported that they can help improve the photocatalytic activity of semiconductors for their SPR effect [31–33]. Some researchers have repoted Au-Bi$_2$O$_3$ composites with enhanced photocatalytic activity, however, using noble metal based materials to treat sewage is quite costed [34,35]. Recently, some researchers found that matallic bismuth had UV-mediated surface plasmon resonance and was a good direct plasmonic photocatalyst [36]. Some of

---

* Corresponding authors.
E-mail addresses: chendaimei@cugb.edu.cn (D. Chen), zhuyf@tsinghua.edu.cn (Y. Zhu).

the photocatalysts modified by metallic bismuth showed enhanced catalytic activity, however, it is necessary to use reducing agents, which is unenvironmetal-friendly [37,38].

Herein, we report a one-pot synthesis of $C/Bi/Bi_2O_3$ composite photocatalyst, using EDTA-Bi as a precursor, which exhibited higher photocatalytic activity than Bi_2O_3 on the degradation of 2,4-DCP under simulated sunlight and visible light irradiation. Reducing agents are not needed in this novel preparation method and it is suitable for mass production.

2. Experimental section

2.1. Material preparation

All chemicals used were reagent grade and used without further purification. The preparation of precursors is as reported [39]. Chart 1 is a flow diagram of the preparation method of samples. 10 ml of nitric acid was added to 290 ml of pure water. 48.51 g (0.1 mol) of $Bi(NO_3)_3 \cdot 5H_2O$ was weighed and added in to the nitric acid solution and dispersed by ultrasonic for 2 h. While strong stirring, 29.22 g (0.1 mol) of ethylenediaminetetraacetic acid (EDTA) were added into the solution above. Ammonium hydroxide is used to regulate the pH of the suspension to 6.5. The resulting suspension was stirred for 2 h, as a result a clear and transparent solution of EDTA-Bi was obtained. Most water was evaporated at 60 °C with the help of the rotary evaporation apparatus. The result solution was kept at 120 °C for 72 h and EDTA-Bi solid was obtained, which is used as the precursor for the preparation of $C/Bi/Bi_2O_3$ composite photocatalyst.

5 g of precursor was weighed and transferred to ceramic crucible and heated to 300 °C and kept at this temperature for 2 h in air. The heating rate was controlled at 4 °C per minute. Other samples were prepared with the same method at 400 °C, 500 °C, 600 °C and the as-prepared samples were named as BiO-300, BiO-400, BiO-500, and BiO-600, respectively.

Bi_2O_3 was prepared as follows: 5 g of $Bi(NO_3)_3 \cdot 5H_2O$ was dried at 60 °C for 4 h and then transferred to ceramic crucible and heated to 600 °C within 150 min and kept at this temperature for 2 h in air. This sample was named Bi_2O_3.

2.2. Characterization of products

In order to identify the material composition and the crystal phase of as-prapared samples, X-ray diffraction (XRD) patterns was abtained from the D/max-2400 X-ray diffractometer (Japan) at 25 °C. 514 nm laser was used to test the Raman spectra of as-prepared samples on a HORIBA HR 800 Laser Confocal Raman Microspectroscopy (Japan). X-ray photoelectron spectroscopy (XPS) of as-prepared samples was obtained from a PHI Quantera XPS (USA). HITACHI SU-8010 cold field emission scanning electron microscope (SEM) (Japan) and HITACHI JEOL2100F thermal field high resolution transmission electron microscope (HRTEM) (Japan) were used to observe the morphology and structure of as-prepared samples. The UV–vis diffuse reflection spectra (DRS) was obtained from a HITACHI U-3900 scan UV–vis spectrophotometer (Japan) using $BaSO_4$ as reference. All electrochemical characterization is obtained from a CH-660D (China) electrochemical work station, using Pt wire as the counter electrode, saturated calomel electrode as the reference electrode and Indium-Tin Oxide (ITO) glass with as-prepared sample films as the working electrodes. The working electrodes were prepared by dispersing 5 mg of as-prepared samples in 500 ml ultra-pure water undersonication for 1 h and then evenly coated on ITO glasses. Then the electrodes were dried in air for 12 h and then heated at 120 °C

in air for 5 h. The light intensity is $50 \, mW/cm^2$ and the distance between the lamp and the electrode is 10 cm.

2.3. Evaluation of photocatalytic activity

The photocatalytic activity of the as-prepared samples was evaluated by the degradation of 2,4-DCP. 500 W xenon lamp was used as light source during the evaluation of catalytic activity and the average light intensity is $35 \, mW/cm^2$. When evaluating visible light catalytic activity, cutoff filter (420 nm) was used and the concentration of 2,4-DCP is 10 mg/L, while it is 20 mg/L when evaluating simulated sunlight catalytic activity and not cutoff was used.

40 mg of sample was weighed and dispersed in 50 ml aqueous solution of 2,4-DCP. Before the light irradiation, the suspensions were first kept in dark and magnetically stirred for 2 h to get to the adsorption–desorption equilibrium. After that, 3 ml of suspension was sampled and the light was turned on. With the light on and magnetically stirring, the photocatalytic reaction lasted for 5 h and 3 ml of suspension was sampled per hour. All suspension was filtered by micropore filter (produced by Jin Teng company and the diameter is $0.45 \, \mu m$). High-performance liquid chromatography (HPLC) (Shimadzu LC-20AT) was adopted to detect the concentration of 2,4-DCP. The mobile phase is methanol and water (volume ratio: 75/25), the elution time was 5.5 min, the flow rate was 1 ml/min, determine wavelength was 284 nm and chromatographic column was a Venusil XBP-C18 (3.9 × 200, Agela Technologies Inc.) column.

3. Results and discussion

3.1. Photocatalytic property

The photocatalytic activity of as-prepared samples was evaluated by the degradation of 2,4-DCP. Fig. 1a and b are the apparent rate constants for 2,4-DCP photocatalytic degradation under visible light irradiation ($\lambda > 420$ nm) and simulated sunlight irradiation. It is obvious that sample BiO-400 has the highest photocatalytic activity and all the prepared samples exhibited higher photocatalytic activity than Bi_2O_3 under simulated sunlight and visible light irradiation ($\lambda > 420$ nm). As shown in Fig. 1c and d, the photodecomposition process of 2,4-DCP under simulated sunlight irradiation was demonstrated by HPLC. The typical HPLC chromatograms in the presence of Bi_2O_3 and BiO-400 were recorded by UV–visible detector. It can be informed that BiO-400 can mineralize 2,4-DCP efficiently, while for Bi_2O_3, the efficiency is much lower (Fig. 1d). No new intermediates or products forms, indicating that degradation process of 2,4-DCP was mineralization rather than ring opening reaction.

3.2. Structure and morphology

XRD is one of the most commonly used research methods for studying the composition of materials, the structure of the atoms, molecules inside the materials or the information of the crystals [40,41]. From the results of Fig. 2a, it can be seen that with the increase of the calcination temperature, the compositions of the products are different. The sample BiO-300 contains α-Bi_2O_3, β-Bi_2O_3, Bi, and some mismatched diffraction peaks in this sample might be the remaining organic compounds. The component of sample BiO-400 is α-Bi_2O_3, Bi and organic carbon (Fig. 2b, c and d). Sample BiO-500 and BiO-600 contain α-Bi_2O_3 and a small amount of organic carbon. As for Bi_2O_3, only the typical diffraction peaks of α-Bi_2O_3 can be detected (Fig. 2b). With the increase of the calcination temperature, the crystallinity of the as-prepared samples increased. BiO-600 has the highest crystallinity, while its
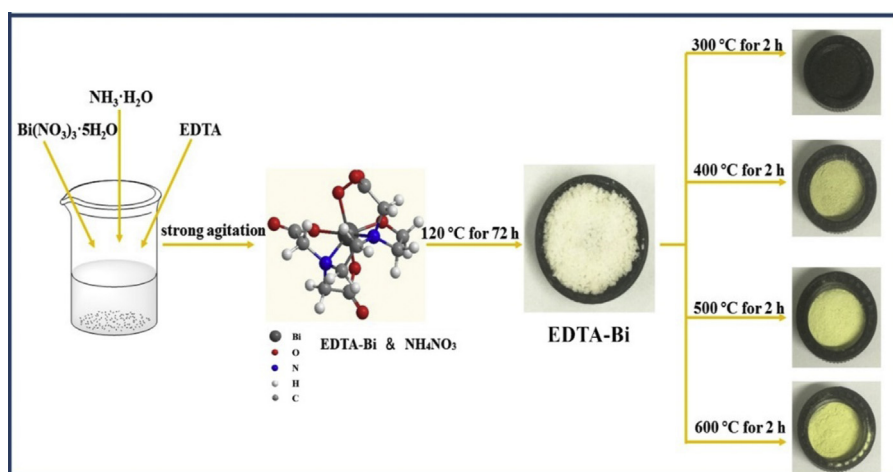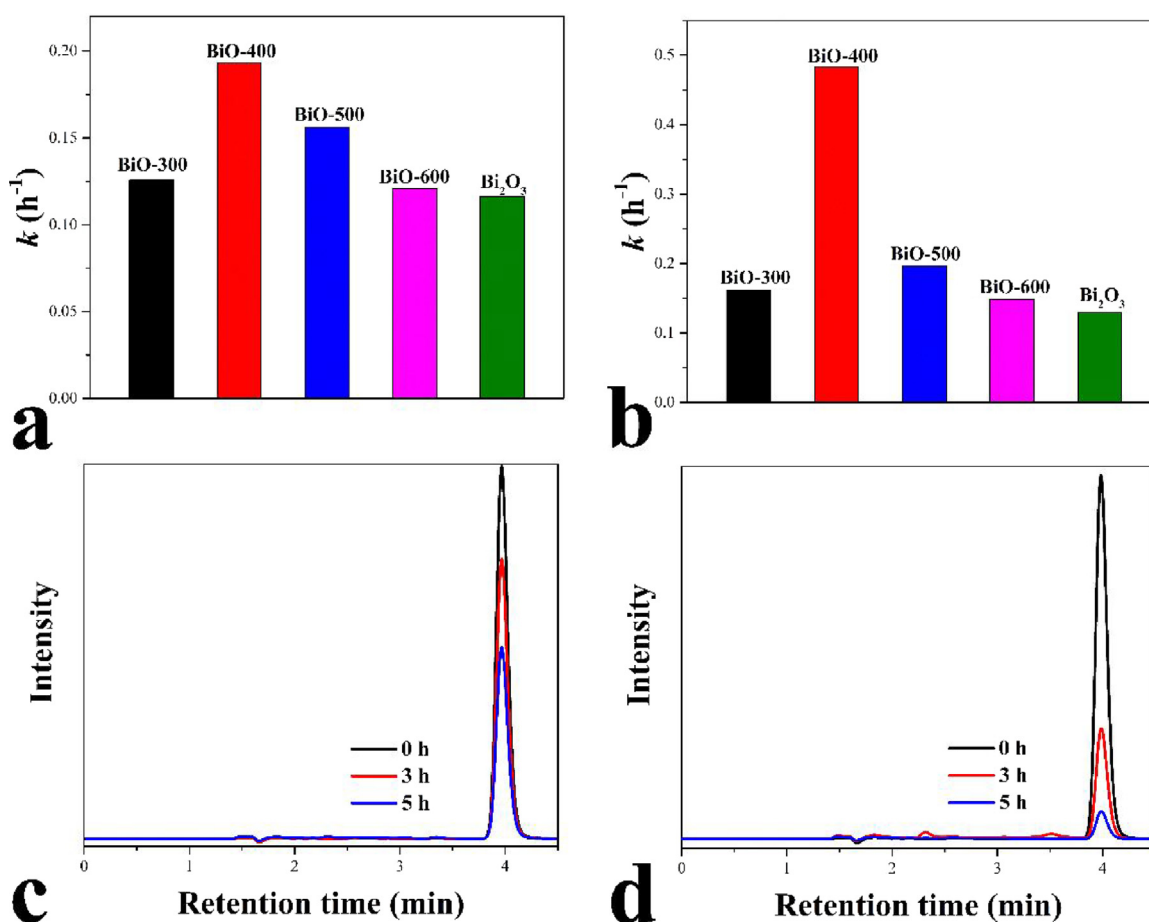
Chart 1. A flow diagram of the sample preparation method.

Fig. 1. Apparent rate constants for 2,4-DCP photocatalytic degradation under visible light irradiation (λ > 420 nm) (a) and simulated sunlight irradiation (b); HPLC results at different irradiation intervals during 2,4-DCP photocatalytic degradation under simulated sunlight irradiation of sample Bi_2O_3 (c) and BiO-400 (d).

photodegradation performance is not the best, indicating that crystallinity is not the key factor for the enhanced activity.

XPS is a method of investigating the surface chemical composition of materials [42]. Fig. 3a the survey spectra of sample BiO-400, BiO-500 and BiO-600, indicating that they consist of C, O and Bi element. All samples consist C, O and Bi, beyond that, sample BiO-300 consists N (Fig. S1). The peaks at 284.8 and 288.8 eV are assigned to C 1 s of the non burned carbon. The peaks at 284.8 eV are assigned to sp^2C atoms of instrument calibration carbon and the peaks at

around 288.8 eV can be assigned to the species of C=O [43]. The peak of C=O in the XPS spectra of sample BiO-400 is stronger than that of BiO-500 and BiO-600, indicating that it contains more remaining organic carbon. As shown in Fig. 3c, the two peaks at 163.8 and 158.5 eV are assigned to Bi $4f_{7/2}$ and Bi $4f_{5/2}$ of Bi_2O_3, while the two small peaks at 161.7 and 156.5 eV are assigned to Bi $4f_{7/2}$ and Bi $4f_{5/2}$ of metallic Bi [44]. It can be inferred that only sample BiO-400 contains metallic Bi, for the other samples do not have the characteristic peaks of metallic Bi. In Fig. 3d, all the samples have two
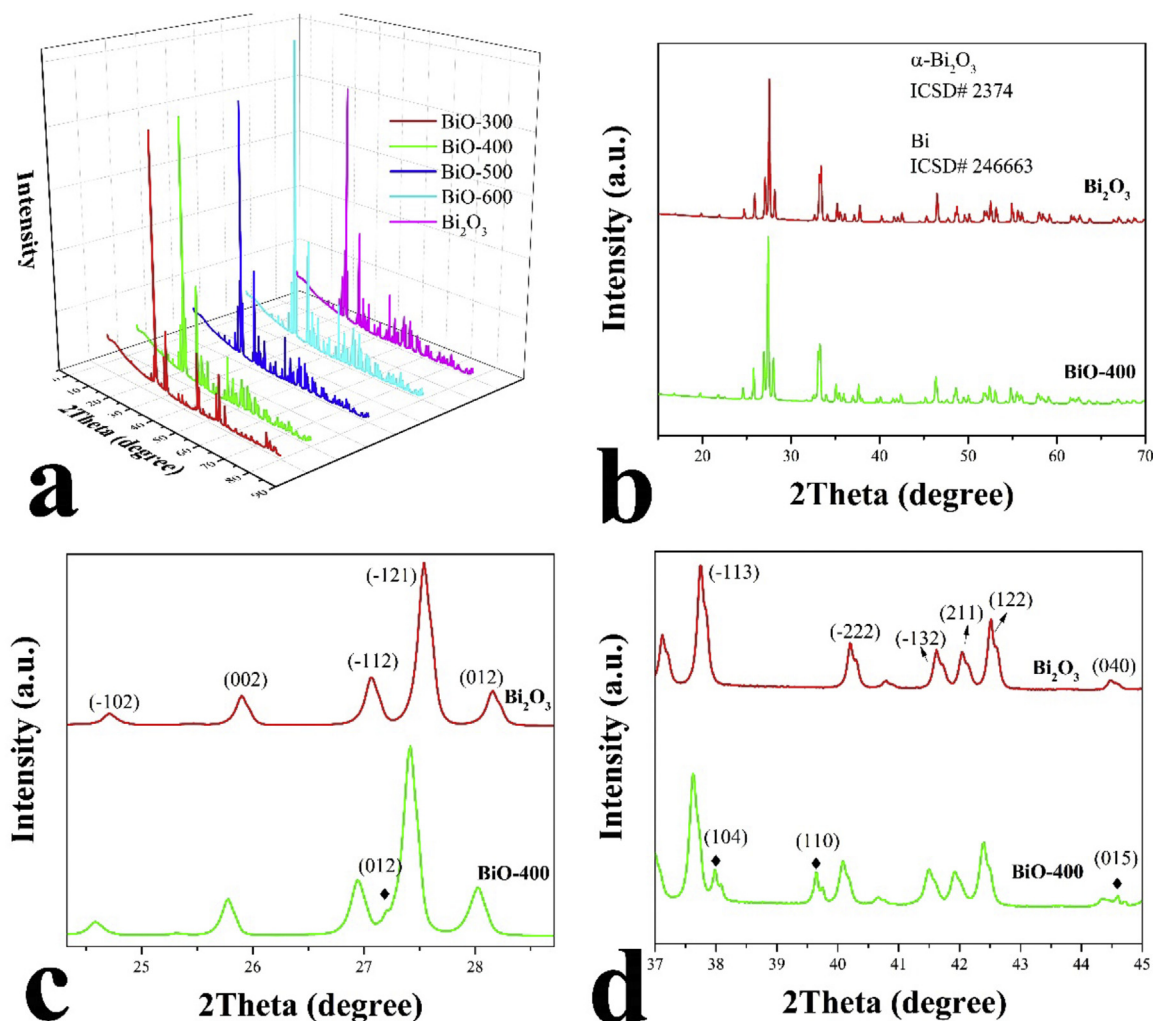
Fig. 2. XRD patterns of prepared samples.

peaks at around 530.0 eV, which are attributed to the formation of Bi–O [45]. The results of XPS spectra show that BiO-400 contains metallic Bi and some remaining organic carbon. This might be a reason for the enhancement of photocatalytic activity.

Raman spectra are often used to detect the vibration and molecular structure of inorganic materials [46]. Fig. 4 is the Raman spectra of as prepared samples. With the increase of preparation temperature, the intensity of Raman spectra improved, indicating that the crystallinity of samples became stronger. For sample BiO-300, three bands exhibited at 109, 296 and 427 cm^{-1} are indexed to Bi-O stretches of β-Bi$_2$O$_3$, [47] while the peaks of α-Bi$_2$O$_3$ are not obvious, indicating that most part of crystalline substance in this sample is β-Bi$_2$O$_3$. For the other samples, the peaks at 117 cm^{-1} are attributed to the vibrations of Bi atoms. The peaks at 137 and 150 cm^{-1} are due to the displacements of both Bi and O atoms. The other peaks at 181, 208, 278, 312, 410 and 445 cm^{-1} are all attributed to vibrations of O atoms. They are all typical Raman spectra of α-Bi$_2$O$_3$ [48–50]. From Fig. 4, it can be inferred that most part of crystalline substance in sample BiO-300 is β-Bi$_2$O$_3$, while for the other samples, they only contain α-Bi$_2$O$_3$.

Fig. 5 shows the SEM images of as-prepared samples. Calcined at 300 °C, the obtained sample shows large bulk structure and it contains a large quantity of metallic Bi and some remaining organic compounds (the insert images in Fig. 5a). When the temperature reached 400 °C, we cannot find remaining organic carbon under SEM (Fig. 3b). It can be seen that the particle size of Bi$_2$O$_3$ is rela-

tively uniform and it is about 200 nm. Calcined at 500 °C, obvious agglomeration occurred to Bi$_2$O$_3$ particles (Fig. 3c). For sample BiO-600, the agglomeration is more serious. As for the Bi$_2$O$_3$ sample, it shows a bulk structure, which does not have a regular morphology or uniform particle size.

TEM and HRTEM images of sample BiO-400 were investigated to further study the microstructure. Fig. 6a confirms that the size of BiO-400 is about 200 nm. In Fig. 6b the lattice spacing of 0.264 nm is corresponded to the (022) plane of the α-Bi$_2$O$_3$. The distinct lattice fringe with a spacing of 0.395 nm can be clearly found in Fig. 6b, corresponding to the (003) plane of metallic Bi. At the edge of this sample, some amorphous structure can be observed, which might be the remaining carbon. Combined with the results of XPS and XRD, the composition of this sample was verified.

3.3. The mechanism for the enhancement of photocatalytic activity

UV–vis DRS is always used to investigate the photophysical properties of materials [51]. Fig. 7 shows the UV–vis DRS of prepared samples. Compared with other samples, BiO-300 and BiO-400 exhibit a broad visible light wave-band absorption because of the presence of remaining organic carbon. With the increase of preparation temperature, the absorption edge of sample BiO-400, BiO-500 and BiO-600 shift to long wavelength direction for the increasing particle size. Compared with sample BiO-600, the
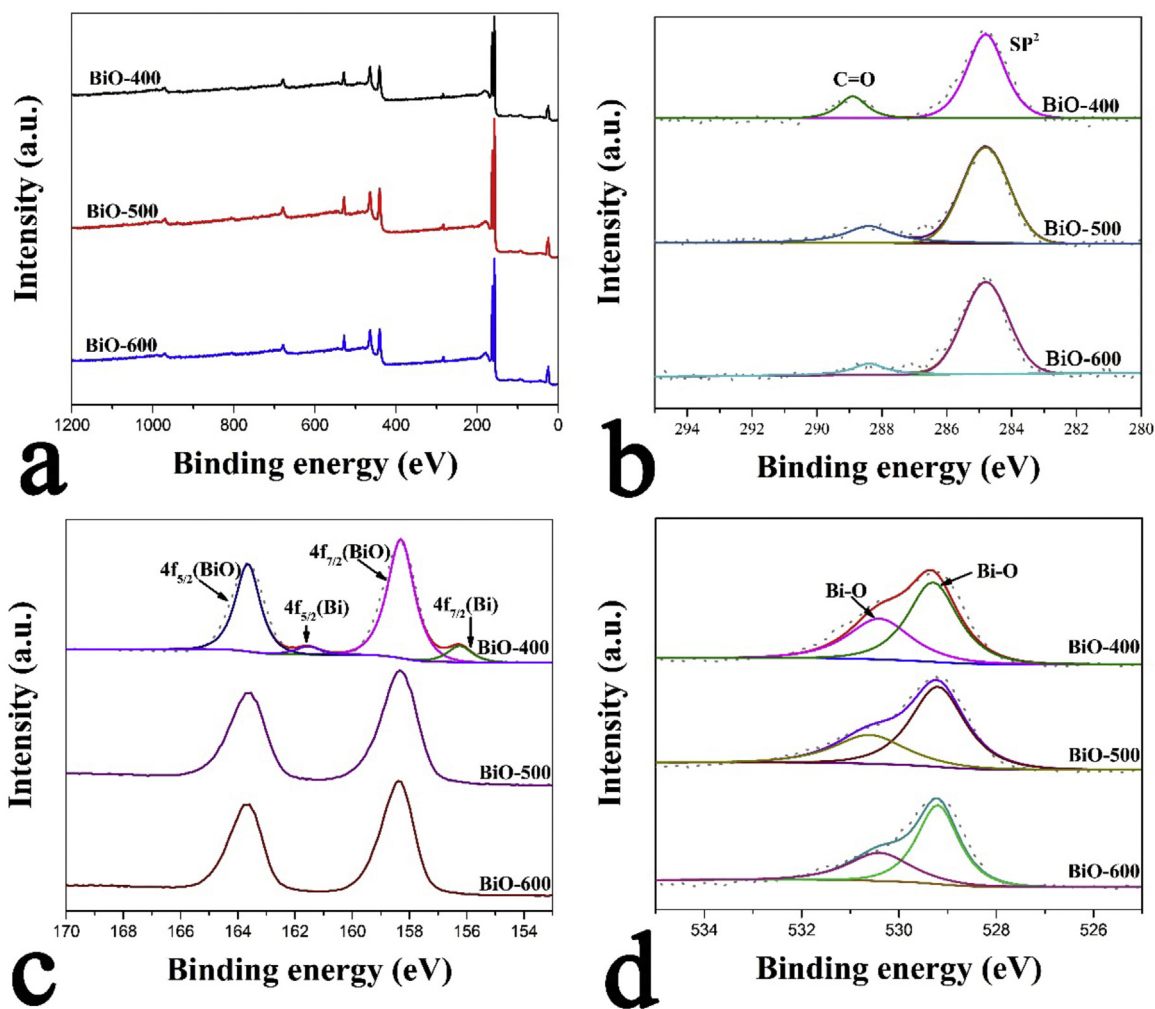
Fig. 3. XPS spectra of the sample BiO-400, BiO-500 and BiO-600: (a) survey spectrum; (b) C 1 s spectrum; (c) Bi 4f spectrum; (d) O 1s.

absorption edge of Bi_2O_3 has a red shift, which is corresponding with its larger particle size. The band gap of BiO-400, BiO-500, BiO-600 and Bi_2O_3 are 2.77, 2.76, 2.74 and 2.70 eV, respectively (Fig. S2).

The specific surface area of the materials is very important for the photocatalytic reaction. Fig. S3 shows the A_{BET} of prepared samples. Sample BiO-300 has the largest A_{BET} due to the large quantity of remaining organic compounds. With the increase of calcination temperature, the content of carbon decreases and the A_{BET} decreases. Compared with Bi_2O_3, the A_{BET} of BiO-400 is 3.03 times higher than that, indicating that there are more active sites in BiO-400, which is crucial for the enhanced photocatalytic activity.

Transient photocurrent and electrochemical impedance spectroscopy (EIS) are always used to investigate the separation efficiency of photogenerated charge carriers [52]. Fig. 8a and b show the transient photocurrent density responses and EIS of prepared-sample electrodes under visible light irradiation, respectively. Sample BiO-400 shows the highest photocurrent response under visible light irradiation (Fig. 8a), which is due to the higher separation efficiency of photogenerated charge carries. Compared with the other samples, sample BiO-300 has the lowest arc radius on the EIS Nyquist plot (Fig. 8b). That is because the large quantity of remaining organic carbon can reduce the resistance of the composites. Except sample BiO-300, the arc radius on the EIS Nyquist plot of the other samples were in accordance with the change of transient photocurrent and photocatalytic activity. Under UV–vis light
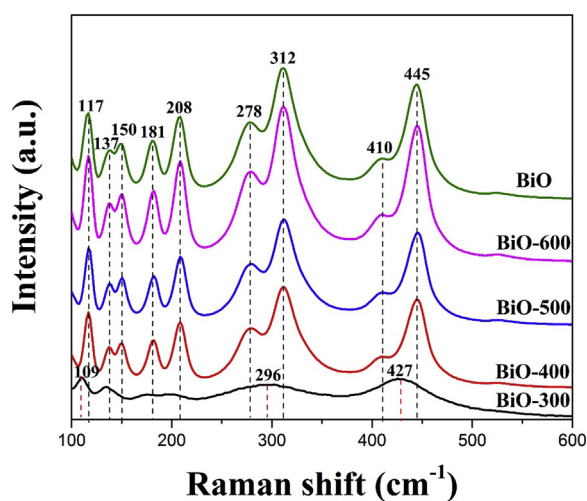

Fig. 4. Raman spectra of prepared samples.

irradiation, the transient photocurrent and arc radius on the EIS Nyquist plot fallow the same to these under visible light (Fig. 8c and d). The results of transient photocurrent and EIS indicate that sample BiO-400 has the highest separation speed of photogenerated charge carries.
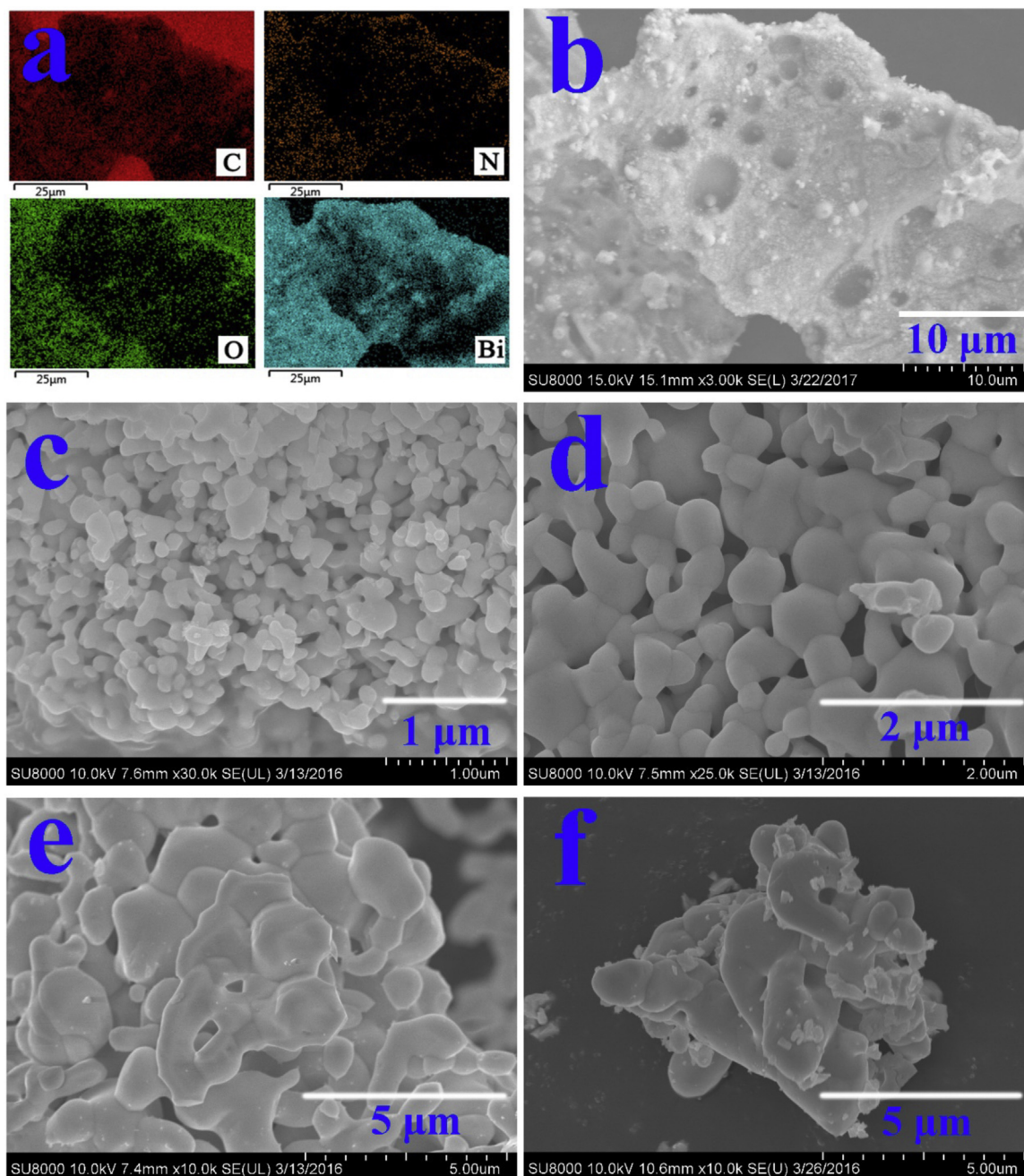
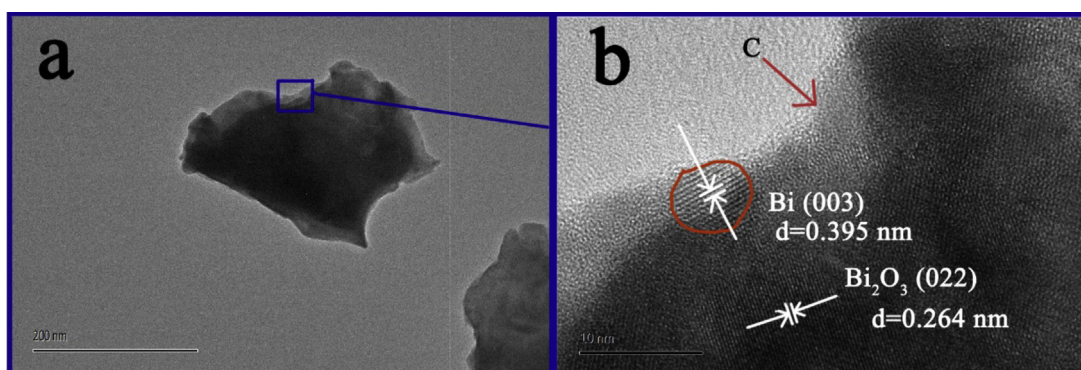**Fig. 5.** SEM-EDX (mapping) of BiO-300 (a), SEM images of sample BiO-300 (b), BiO-400.

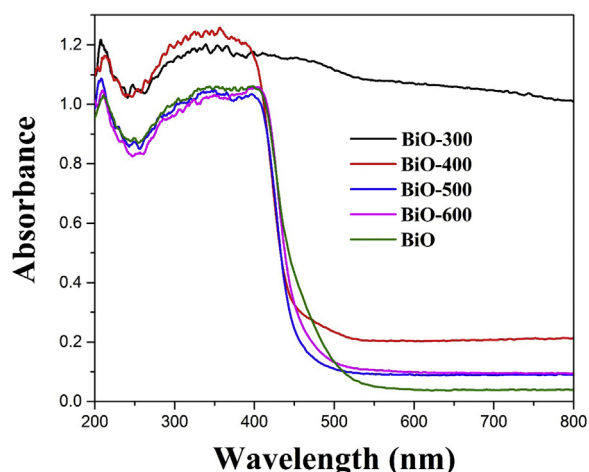**Fig. 6.** TEM and HRTEM images of sample BiO-400 (b), BiO-500 (d), BiO-600 (e) and Bi₂O₃ (f).

Fig. 7. UV–vis diffuse reflectance spectra of prepared samples.

Fig. 9. Photoluminescence spectra of sample 400 and Bi₂O₃.

To further investigate the recombination progress and transfer efficiency of photoproduced electron-hole pairs, Photoluminescence (PL) spectra of BiO-400 and Bi₂O₃ was employed. It is clear that the PL intensity of BiO-400 is much lower than that of Bi₂O₃, indicating that the relaxation of a fraction of sample 400 excitons may occur via charge transfer of electrons and holes rather than radiative paths. Thus, it can be inferred that the sample BiO-400 has lower recombination probability of photogenerated charge carriers compared with Bi₂O₃ (Fig. 9).
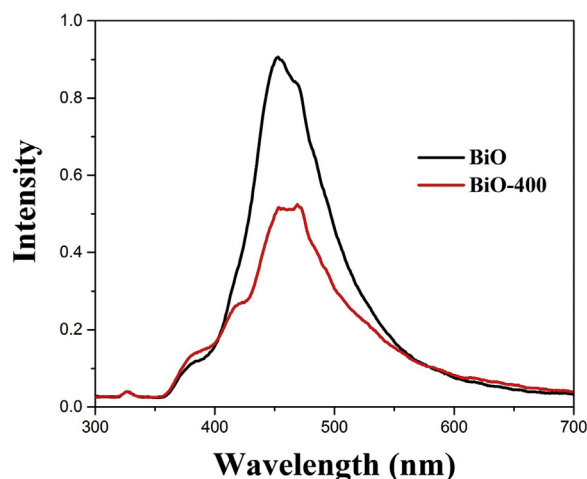
To investigate the respective impact of photoactive radical species on the degradation of 2,4-DCP over prepared samples under visible light and UV–vis light irradiation, the trapping experiments using different radical scavengers were performed, which is helpful for understanding the under-lying photocatalytic reaction mechanism. The addition of N_2 is used to remove the oxygen and prevent the formation of superoxide radicals. Isopropyl alcohol (IPA) is a scavenger for hydroxyl radicals, and sodium sulfite (Na_2SO_3) is a scavenger for holes. Fig. 10a and b are the photocatalytic activity
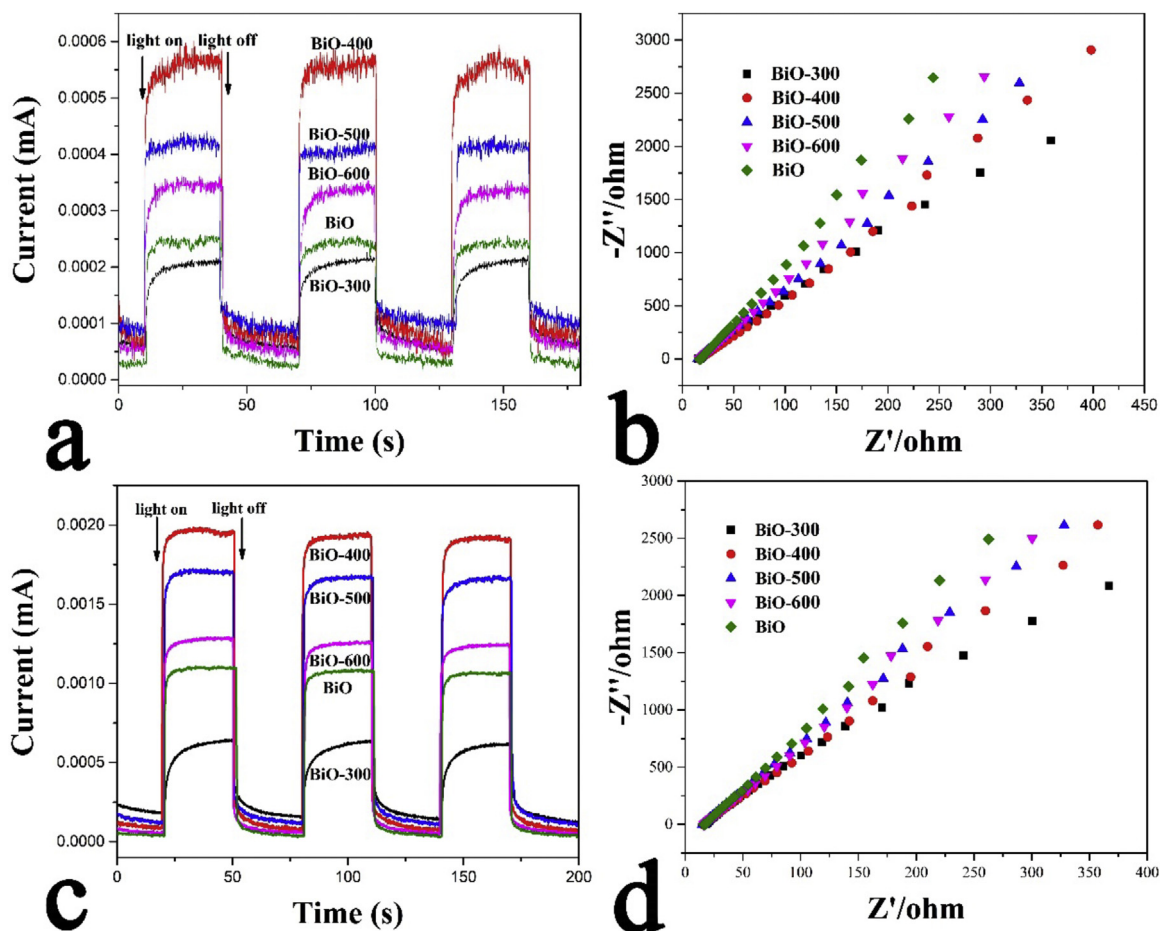

Fig. 8. The transient photocurrent density responses of prepared-sample electrodes with light on/off cycles under visible light irradiation (λ > 420 nm) (a) and UV–vis light irradiation (c). EIS Nyquist plots of prepared-sample electrodes under visible light irradiation (λ > 420 nm) (b) and UV–vis light irradiation (d).
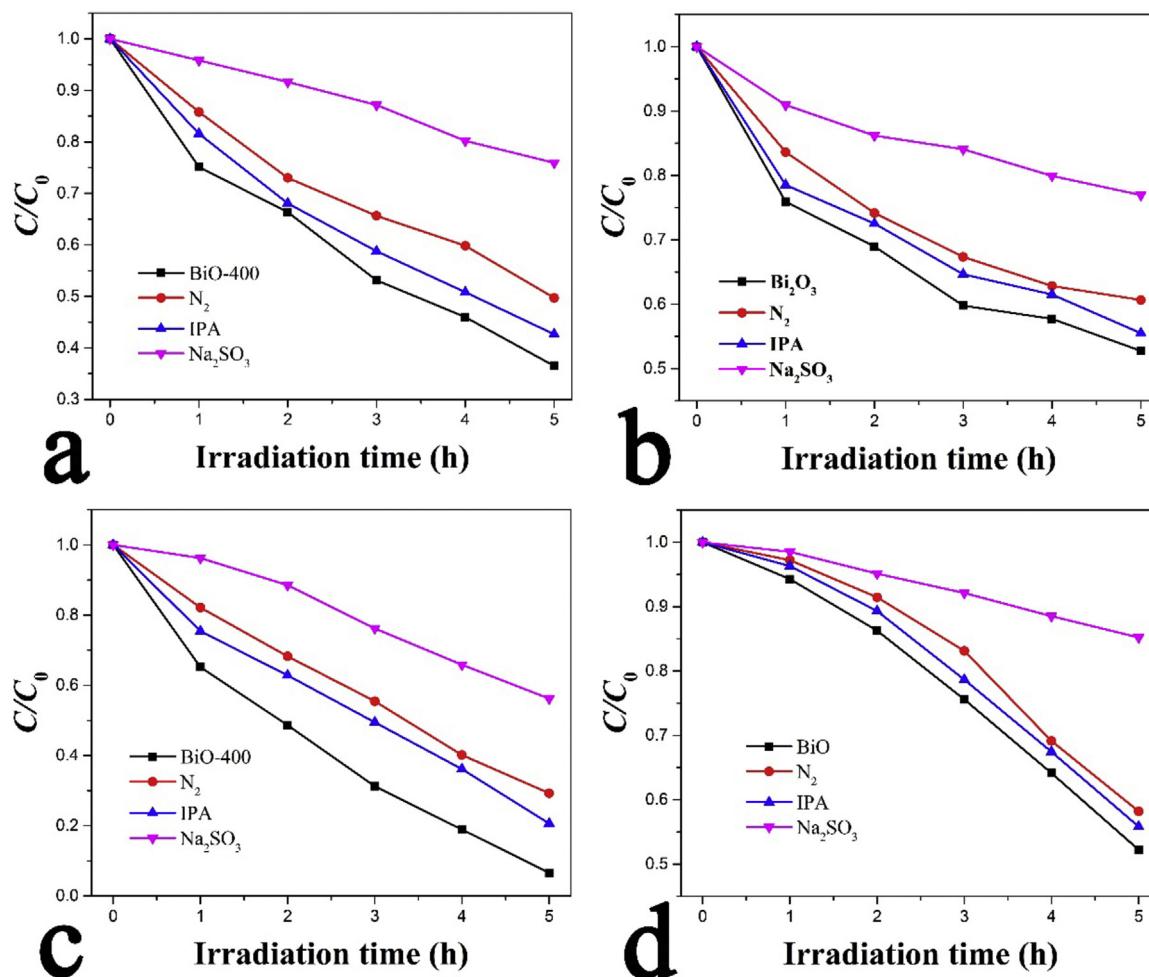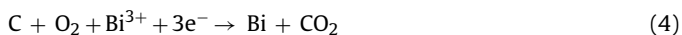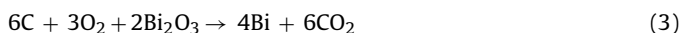
Fig. 10. The photocatalytic activity of sample BiO-400 with radical scavengers on the degradation of 2,4-DCP under visible light (Fig. 10a) and UV–vis light irradiation (Fig. 10c). The photocatalytic activity of Bi_2O_3 with radical scavengers on the degradation of 2,4-DCP under visible light (Fig. 10b) and UV–vis light irradiation (Fig. 10d).

of sample BiO-400 and Bi_2O_3 with radical scavengers on the degradation of 2,4-DCP under visible light irradiation. The addition of Na_2SO_3 can strongly influence the photocatalytic activity of both sample BiO-400 and Bi_2O_3, while IPA and N_2 only have a little influence on degradation efficiency, indicating that under visible light irradiation, the main active species of sample BiO-400 and Bi_2O_3 are both holes. Under UV–vis light irradiation, the main active species of sample BiO-400 and Bi_2O_3 are still holes, while for sample BiO-400, the effect of superoxide radicals are stronger than that of Bi_2O_3, which is probably caused by the SPR effect of metallic Bi.
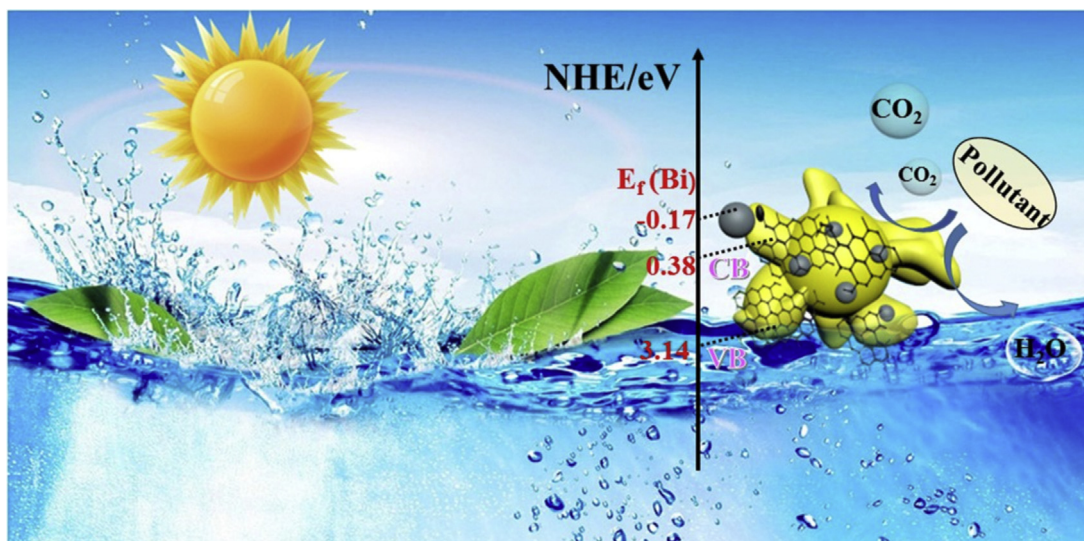
Based on the above results, the formation mechanism of $Bi/Bi_2O_3/C$ composite photocatalyst was presented. In the precursor EDTA-Bi, bismuth ions are firmly bounded in the center of EDTA, just like being locked in a cage made of C, H, O, and N elements. Calcined in air, the structures of EDTA-Bi are damaged and the following reactions can occur.

$$2Bi^{3+} + 3O_2 + 6e^- \rightarrow 2Bi_2O_3 \tag{1}$$

$$C + O_2 \rightarrow CO_2\uparrow \tag{2}$$

$$6C + 3O_2 + 2Bi_2O_3 \rightarrow 4Bi + 6CO_2 \tag{3}$$

$$C + O_2 + Bi^{3+} + 3e^- \rightarrow Bi + CO_2 \tag{4}$$

Carbon has reducibility. At 300 °C, the remaining organic carbon can participate in reactions (3) and (4) and metallic Bi is produced. Due to the low temperature, most part of Bi_2O_3 in this sample is β-Bi_2O_3 and the crystallinity is not high. Calcined at 400 °C, β-Bi_2O_3

all transfered to α-Bi_2O_3 and the phenomenon of agglomeration appeared in the Bi_2O_3 particles. Because most carbon become CO_2 (2) and a samll amount of remaining organic carbon can participate in reaction (3) and (4), BiO-400 contains some metallic Bi. From the results of DRS and XPS, it can be infered that sample BiO-500 and BiO-600 still contain a little amount of remaining organic carbon. Because most carbon bacame CO_2 under high temperature, it is hard for reaction (3) and (4) to occur, as a result the components of sample BiO-500 and BiO-600 are Bi_2O_3 and carbon. With increasing calcined temperature, the crystallinity of Bi_2O_3 becomes higher and the particle size of particles becomes larger.

Herein, a schematic diagram of photogenerated electron-hole pair separation and a possible mechanism of $C/Bi/Bi_2O_3$ composite photocatalyst was proposed (Scheme. 1). Under light irradiation, the electrons on the VB of Bi_2O_3 are excited and transfer to the CB, where it can react with O_2 and generate superoxide radicals. When electrons are excited, holes are produced on the VB. Both superoxide radical and hole are active species and have strong oxidation ability. In virtue of the SPR effect of metallic Bi, the composite has stronger light absorption and high separation efficiency of photogenerated electron-hole pairs. More importantly, the Fermi level of metallic Bi is −0.17 eV, which is much more negative than the CB of Bi_2O_3, therefore photogenerated electrons can transfer to the CB of Bi_2O_3 and the amount of superoxide radicals is increased. Besides, BiO-400 has stronger absorption due to the production of remaining organic carbon form EDTA, which provides an efficiency path for electron transfer. Meanwhile, the smaller particle size and

Scheme 1. Schematic diagram of the proposed mechanism for the degradation of organic pollutants over the C/Bi/Bi$_2$O$_3$ composite under visible light and UV–vis light irradiation.

enhanced A_{BET} provide more active sites benefiting to the inter reactions. Benefiting from the above-mentioned advantages, the C/Bi/Bi$_2$O$_3$ composite photocatalyst shows higher photocatalytic activity.

4. Conclusion

In this work, a novel C/Bi/Bi$_2$O$_3$ composite photocatalyst was prepared by a facile one-pot method, using EDTA-Bi as a precursor. Compared with Bi$_2$O$_3$, the obtained samples showed enhanced photocatalytic activity under both simulated sunlight and visible light irradiation on the degradation of 2,4-DCP. The remaining organic carbon can enhance the visible light absorption of the composite, which is beneficial to the photocatalytic activity. The SPR effect of metallic Bi can help to generate more active photoexcitons and accelerate the separation of electron-hole pairs. These findings open up a new access to the preparation of highly efficient C/Bi/Bi$_2$O$_3$ composite materials without using reduction agent, which is suitable for mass production.

Acknowledgements

Appendix A. Supplementary data

Supplementary data associated with this article can be found, in the online version, at http://dx.doi.org/10.1016/j.apcatb.2017.07.030.

References

[1] W. Wang, D. Xu, B. Cheng, J. Yu, C. Jiang, J. Mater. Chem. A 5 (2017) 5020–5029.
[2] D. Chen, D. Yang, A. Qun Wang, Z. Jiang, Ind. Eng. Chem. Res. 45 (2006) 4110–4116.
[3] K. Guo, Z. Liu, C. Zhou, J. Han, Y. Zhao, Z. Liu, Y. Li, T. Cui, W. Bo, Z. Jing, App. Catal. B 154 (2014) 27–35.
[4] Z. Liu, K. Guo, J. Han, Y. Li, T. Cui, B. Wang, J. Ya, C. Zhou, Small 10 (2014) 3153–3161.
[5] J. Han, Z. Liu, K. Guo, W. Bo, X. Zhang, T. Hong, App. Catal. B 163 (2015) 179–188.
[6] D. Chen, K. Wang, D. Xiang, R. Zong, W. Yao, Y. Zhu, App. Catal. B 147 (2014) 554–561.
[7] J. Yu, X. Yu, Environ. Sci. Technol. 42 (2008) 4902–4907.
[8] Z. Wei, Y. Liu, J. Wang, R. Zong, W. Yao, J. Wang, Y. Zhu, Nanoscale 7 (2015) 13943–13950.
[9] H. Xu, Y. Xu, H. Li, J. Xia, J. Xiong, S. Yin, C. Huang, H. Wan, Dalton Trans. 41 (2012) 3387–3394.
[10] D. Chen, K. Wang, W. Hong, R. Zong, W. Yao, Y. Zhu, App. Catal. B 166 (2015) 366–373.
[11] Q. Hao, X. Niu, C. Nie, S. Hao, W. Zou, J. Ge, D. Chen, W. Yao, Phys. Chem. Chem. Phys. 18 (2016) 31410–31418.
[12] Z. Wei, F. Liang, Y. Liu, W. Luo, J. Wang, W. Yao, Y. Zhu, App. Catal. B 201 (2017) 600–606.
[13] J. Wang, L. Tang, G. Zeng, Y. Deng, Y. Liu, L. Wang, Y. Zhou, Z. Guo, J. Wang, C. Zhang, Appl. Catal. B 209 (2017) 285–294.
[14] Q. Xiang, J. Yu, M. Jaroniec, J. Phys. Chem. C 115 (2011) 7355–7363.
[15] C. Pulgarin, J. Kiwi, Langmuir 11 (1995) 519–526.
[16] D.G. Shchukin, E.A. Ustinovich, D.V. Sviridov, A.I. Kulak, High Energy Chem. 38 (2004) 167–173.
[17] S. Ikeda, T. Itani, K. Nango, M. Matsumura, Catal. Lett. 98 (2004) 229–233.
[18] J. Zhang, H. Ma, Z. Liu, App. Catal. B 201 (2017) 84–91.
[19] M.A. Shoeib, O.E. Abdelsalam, M.G. Khafagi, R.E. Hammam, Adv. Powder Technol. 23 (2012) 298–304.
[20] A. Zhang, N. Zhang, S. Hong, M. Zhang, Kinet. Catal. 50 (2009) 748–751.
[21] S. Li, S. Hu, K. Xu, W. Jiang, J. Liu, Z. Wang, Nanomaterials 7 (2017) 22.
[22] Y. Guo, X. Lou, D. Xiao, L. Xu, Z. Wang, J. Liu, J. Hazard. Mater. 241–242 (2012) 301–306.
[23] X. Zhang, L. Zhang, T. Xie, D. Wang, J. Phys. Chem. C 113 (2009) 7371–7378.
[24] W. Wang, F. Huang, X. Lin, J. Yang, Catal. Commun. 9 (2008) 8–12.
[25] S. Sood, A. Umar, S.K. Mehta, S.K. Kansal, Ceram. Int. 41 (2014) 3355–3364.
[26] P.Y. Ayekoe, D. Robert, D.L. Goné, Environ. Chem. Lett. 13 (2015) 327–332.
[27] P. Lv, P. Zheng, X. Wang, F. Huang, J. Alloy Compd. 45 (2014) 285–290.
[28] T. Xie, C. Liu, L. Xu, J. Yang, W. Zhou, J. Phys. Chem. C 117 (2013) 24601–24610.
[29] Y. Li, J. Wang, H. Yao, L. Dang, Z. Li, Catal. Commun. 12 (2011) 660–664.
[30] X. Fan, N. Hua, H. Jia, Y. Zhu, Z. Wang, J. Xu, C. Wang, Sci. Adv. Mater. 6 (2014) 1892–1899.
[31] Y.H. Tseng, I.G. Chang, Y. Tai, K.W. Wu, J. Nanosci. Nanotechnol. 12 (2012) 416–422.
[32] E. Liu, L. Kang, Y. Yang, T. Sun, X. Hu, C. Zhu, H. Liu, Q. Wang, X. Li, J. Fan, Nanotechnology 25 (2014) 165401.
[33] K. Ullah, A. Ali, S. Ye, L. Zhu, W.C. Oh, Sci. Adv. Mater. 7 (2015) 606–614.
[34] S. Anandan, G.J. Lee, P.K. Chen, C. Fan, J.J. Wu, Ind. Eng. Chem. Res. 49 (2014) 9729–9737.
[35] H.Y. Jiang, K. Cheng, J. Lin, Phys. Chem. Chem. Phys. 14 (2012) 12114–12121.
[36] F. Dong, T. Xiong, Y. Sun, Z. Zhao, Y. Zhou, X. Feng, Z. Wu, Chem. Commun. 50 (2014) 10386–10389.
[37] S. Yu, H. Huang, F. Dong, M. Li, N. Tian, T. Zhang, Y. Zhang, ACS Appl. Mater. Interface 7 (2015) 27925–27933.
[38] J. Wang, L. Tang, G.M. Zeng, Y.N. Liu, Y.Y. Zhou, Y.C. Deng, J.J. Wang, B. Peng, ACS Sustain. Chem. Eng. 5 (2017) 1062–1072.
[39] D. Li, M. Gu, Q.-G. Zhong, J. Synth. Cryst. 12 (2013) 015 (in Chinese).
[40] Q. Xiang, J. Yu, M. Jaroniec, J. Am. Chem. Soc. 134 (2012) 6575–6578.
[41] S. Liu, J. Yu, M. Jaroniec, J. Am. Chem. Soc. 132 (2010) 11914–11916.

[42] M.C. Pham, A. Hachemi, M. Delamar, J. Electroanal. Chem. 184 (1985) 197–203.
[43] D. Zhan, Z. Ni, W. Chen, L. Sun, Z. Luo, L. Lai, T. Yu, A.T.S. Wee, Z. Shen, Carbon 49 (2011) 1362–1366.
[44] Xiangwen, Huaqiang, Jiefu, Nano Res. 4 (2011) 470–482.
[45] J.F. Moulder, J. Chastain, R.C. King Jr., Chem. Phys. Lett. 99 (1992) 7–10.
[46] C. Jiang, P. Zhang, B. Zhang, J. Li, M. Wang, Ozone Sci. Eng. 35 (2013) 308–315.
[47] F.D. Hardcastle, I.E. Wachs, J. Solid State Chem. 97 (2002) 319–331.

[48] G.S. Devi, J. Electrochem. Soc. 145 (1998) 1039–1044.
[49] L. Kumari, J.H. Lin, Y.R. Ma, J. Phys. Condens. Matter 19 (2007) 406204.
[50] V.N. Denisov, A.N. Ivlev, A.S. Lipin, B.N. Mavrin, V.G. Orlov, J. Phys. Condens. Matter 9 (1999) 4967–4978.
[51] Q. Hao, S. Hao, X. Niu, X. Li, D. Chen, H. Ding, Chin. J. Catal. 38 (2017) 278–286.
[52] D. Chen, Q. Hao, Z. Wang, H. Ding, Y. Zhu, CrystEngComm 18 (2016) 1976–1986.